1	Role of Subauroral Polarization Streams in Deep Injections of
2	Energetic Electrons into the Inner Magnetosphere
3	
4	R Goyal ¹ , H Zhao ¹ , S Califf ² , J Goldstein ³ and T E Sarris ⁴
5	
6	¹ Department of Physics, Auburn University, Auburn, Alabama, USA
7	² CIRES, University of Colorado Boulder, Boulder, CO, USA
8	³ Southwest Research Institute, San Antonio, TX, USA
9 10	⁴ Department of Electrical and Computer Engineering, Democritus University of Thrace, Xanthi, Greece
11	Corresponding author: Ravinder Goyal (<u>rzg0081@auburn.edu</u>)
12	
13	
14	Key points
15	• A moderate storm on 2015-09-07 injected energetic charged particles into Earth's lower L* (\leq
16	4).
17	• The electric fields generated by subauroral polarization streams (SAPS) are a potential cause
18	behind these deep injections.
19	• The quantitative fitting of the SAPS model to Van Allen Probes observations highly affects the
20	simulated lower energy electron fluxes.
21	
22	
23	
24	
25	
26	
27	
28	
29	

Abstract

30

42

52

53

54

55

56

57

58

59

The electric fields of subauroral polarization streams (SAPS) have been suggested to affect 31 32 energetic charged particles' dynamics in the inner magnetosphere, though their role on radiation belt electrons has never been properly quantified. A moderate geomagnetic storm on 2015-09-07 33 caused the deep injection of 10s -100s of keV electrons in Earth's inner magnetosphere to low L* 34 $(L^* < 4)$. Using a 2-D test particle tracer, we present the effects of electric fields given by the 35 Volland-Stern model, a SAPS (Goldstein et al., 2005) model, and a modified SAPS model on the 36 energetic electron deep injections. The modified SAPS model reflects the SAPS electric field 37 observations by the Van Allen Probes and is supported by Defense Meteorological Satellite 38 Program (DMSP) observations. Simulations suggest that the SAPS electric field pushes 10-2039 MeV/G electrons Earthward to L*~2.7 in 2.5 hours, much deeper compared to the Volland-Stern 40 electric field. 41

Plain Language Summary

The study of energetic charged particle dynamics in Earth's inner magnetosphere is important as 43 44 these charged particles pose a danger to the human technology systems (satellites, etc.) traversing through the region. The moderate to intense geomagnetic storms cause added complexity by 45 transporting these charged particles into and out of the inner magnetospheric region. To understand 46 this complexity, a study is conducted using Van Allen Probe observations for a moderate storm on 47 2015-09-07 which pushed 10s – 100s of keV electrons deep into Earth's inner magnetosphere. It 48 is suggested that the electric fields generated due to Subauroral Polarization Streams (SAPS) are 49 one of the major causes behind such deep injections, and that SAPS cause lower energy electrons 50 to penetrate deeper into the inner magnetosphere than higher energy electrons. 51

1. Introduction

Earth's radiation belts are zones with large fluxes of energetic charged particles and consisting of outer and inner belts, with the in-between slot region having much lower fluxes (e.g., Lyons and Thorne, 1973; Millan and Baker, 2012). The particles within the radiation belts represent one of the most widespread and enduring hazards encompassed by what we collectively name as space weather (Baker and Lanzerotti, 2016). Understanding these highly dynamic zones has been opened up as a new challenge with the launch of the Van Allen Probes (Mauk et al., 2012; Kessel et al., 2013). Observations have shown that the energetic charged particles are frequently pushed to very

deep regions of Earth's inner magnetosphere during geomagnetic active times (Reeves et al., 2016; Zhao et al., 2017, 2023; Califf et al., 2022). Different mechanisms such as interplanetary shock induced electric fields, radial diffusion, substorm-related injections, and enhanced convection electric fields have been proposed as driving causes for such deep injections. The interplanetary shock induced electric fields energize the charged particles, but high intensity shocks capable of causing such energization at low L-shells rarely occur (e.g., Kanekal et al., 2016; Li et al., 1993). Fast transport into $L^* < 4$ by substorms also does not occur frequently (e.g., Turner et al., 2015). Research has suggested that short-lived increases in the convection electric field can account for enhancements of electrons in the 100s of keV range at lower L-shells (Califf et al. 2017; Su et al. 2016). Zhao et al. (2017) suggested a localized DC electric field as a potential mechanism to explain the observed MLT distributions of electrons and differential deep injections between protons and electrons, where electrons systematically reach lower L* than protons with similar energies. Based on Defense Meteorological Satellite Program (DMSP) and Van Allen Probes observations, Lejosne et al. (2018) have shown the strong correlation between deep injections of energetic electrons and the Subauroral Polarization Streams (SAPS) and attributed it to SAPS's significant electric potential drop of several tens of kilovolts in the pre-midnight sector.

Foster and Burke (2002) introduced the term 'SAPS' for a mechanism with large latitudinal extents (Yeh et al., 1991), long durations polarization jets (PJ) (Galperin et al., 1974) and Subauroral ion drifts (SAID) (Spiro et al., 1979). SAPS typically manifest at storm onset, flowing westward, and exhibits strong correlations with geomagnetic indices, as noted in previous works by Foster (1993) and Foster & Vo (2002). Based on Combined Release and Radiation Effects Satellite (CRRES) data, Rowland and Wygant (1998) discovered an unexpected increase in the duskward electric field within L = 3.5 - 5.5 in the evening sector during active periods (Kp > 3). This behavior contradicted the predictions made by empirical models such as Volland-Stern (VS) model (Volland, 1973; Stern, 1975). This enhancement was later linked to SAPS electric fields, underscoring their importance in shaping the overall electric field dynamics in the inner magnetosphere. Furthermore, Califf et al. (2014), based on four years of Time History of Events and Macroscale Interactions during Substorms (THEMIS) data, provided a complete picture of dawn-dusk electric field with a full MLT coverage in the inner magnetosphere. Their results strongly agree with the CRRES results from Rowland and Wygant (1998) on the duskside.

In the present study, we demonstrate the role of SAPS electric fields on deep injections of energetic electrons during the 2015-09-07 geomagnetic storm using test particle simulations. Our study uses an Hp-driven version of the VS model, combined with an Hp-driven model for SAPS derived from statical averages of ground-based radar data (Goldstein et al., 2005). A quantitative modification to the SAPS model fitted to event-specific electric field observations from the Van Allen Probes is also conducted. The results under different electric field models are compared, and the role of SAPS electric fields on energetic electron deep injections is revealed quantitatively for the first time.

2. Observations

A moderate geomagnetic storm on 2015-09-07 with Kp index reaching 6+ and Dst (Disturbance Storm Time) index attaining a minimum of -72 nT disturbed Earth's radiation belt particle fluxes.

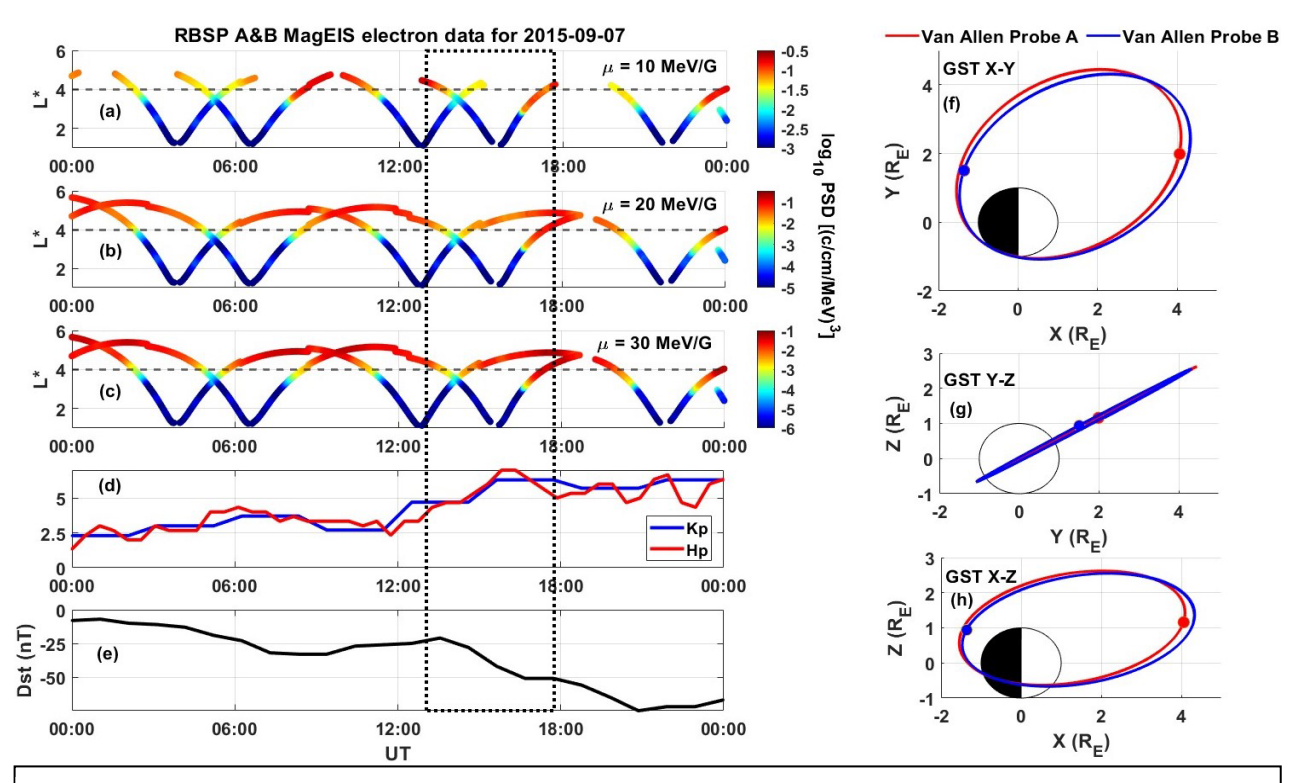


Figure 1 Phase space density variations as a function of L* and time on 2015-09-07 for μ = (a) 10 MeV/G (b) 20 MeV/G (c) 30 MeV/G, K = 0.1 G^{1/2}R_E electrons. Panel (d) shows the Kp and Hp indices and panel (e) shows the Dst index. The dotted black box highlights the two probes' passes during which the PSD enhancements are observed at L*~3 – 4. Panels (f) – (h) present the spacecraft trajectories in GSE coordinate system on 2015-09-07.

Figure 1(a) – 1(c) show the electron phase space density (PSD) variations as a function of L* on this day, for populations with different first adiabatic invariants, (a) $\mu = 10$ MeV/G, (b) $\mu = 20$

correspond to 10s - 100s of keV electrons at L*~2-5. The PSD is calculated using Magnetic Electron Ion Spectrometer (MagEIS) observations (Blake et al., 2013; Claudepierre et al., 2021) under the T89D (Tsyganenko, 1989) external magnetic field model using the method described by Chen et al. (2005). Figure 1(d) shows the Kp & Hp30 (a Kp-like index with a time resolution of half an hour; Yamazaki et al., 2022) indexes and Figure 1(e) shows the Dst index for 2015-09-07. Figure 1(f)-1(h) show the Van Allen Probes' trajectories in GSE coordinates. The Van Allen Probes' apogees were in the pre-dusk sector, and the probes were located near noon during outbound passes and near dusk during inbound passes. During the consecutive outbound passes between 14 and 18 UT (shown as the rectangular box), Van Allen Probes observed the electron PSD enhanced by over an order of magnitude at $L^* \sim 3 - 4$ within 3 hours, which is more apparent for lower energy electrons, showing fast, deep injections of 10s - 100s of keV electrons. The deep injection of electrons is defined as the daily-averaged PSD increasing by at least a factor of 2 within a day over $\Delta L^* \ge 0.5$ at $L^* < 4$ (Zhao et al., 2023). Such deep injections cause flux enhancement at very low radial locations (e.g., Hua et al., 2019). During the inbound pass shortly after these observations, Probe-A observed an enhanced radial electric field (outward from the Earth, perpendicular to the ambient magnetic field) using two pairs of spherical double probe sensors (Wygant et al., 2013) at $L^*\sim 3-4$, (Figure 2(a) black curve). These observed electric fields during this event, along with observations of 1-50 keV electron and proton fluxes and plasma density, have been reported by Califf et al. (2022) and identified as SAPS electric fields. These enhanced SAPS electric fields below L*~ 4 spatially coincided with the deep injections of energetic electrons shown in Figure 1. The deep injection event that occurred between ~ 14:00 UT and 17:00 UT was observed by the Van Allen Probes during outbound passes. However, the SAPS features were observed by the Probes later during their inbound passes near dusk. Due to the limited spatiotemporal coverage of the Van Allen Probes, it is not immediately clear whether SAPS were present at the dusk sector during electron injections, which motivated us to make use of Low-Earth-orbit (LEO) DMSP observations. Figure 2(b) shows the horizontal ion drift velocities measured by the DMSP, which indicates westward SAPS flow velocity (Foster and Vo 2002), during 20:20 - 20:30 UT, around the time of observations of SAPS by Probe - A. L* is calculated by mapping DMSP's location to the magnetic equator using the T89D magnetic field model. The DMSP observations show elevated horizontal ion drift velocities at $L^*\sim 3-4$, showing the presence of SAPS at these spatial

MeV/G, (c) $\mu = 30$ MeV/G and the second adiabatic invariant K = 0.1 G^{1/2}R_E. These primarily

103

104

105

106

107

108

109

110

111

112

113

114

115

116

117

118

119

120

121

122

123

124

125

126

127

128

129

130

131

132

133

locations. This is consistent with Van Allen Probes observations of SAPS near the magnetic equator. Leveraging the higher spatiotemporal resolution of LEO observations, the DMSP observations in the dusk sector during the electron injections were also studied. Figure 2(c) shows one example: during 16:45 – 17:02 UT, around the time of deep injections of energetic electrons, enhanced horizontal ion drifts at low L* were also observed by DMSP. These observations indicate that SAPS were present during the fast, deep injections of energetic electrons.

140

141

134

135

136

137

138

139

3. Electric field models

We use a 2D particle tracer combined with the SAPS electric field model to study the effect of 142 SAPS electric fields on electron populations of different energies. We use Goldstein et al. (2005) 143 model for the SAPS electric field; for the convection electric field, we use the VS model. The VS 144 model represents a symmetrical convection electric field through the electric potential $U(r, \phi)$ = 145 $-\frac{a}{r} - br^{\gamma} sin\phi$. Here, r denotes the equatorial distance from the Earth's center, and ϕ represents 146 the azimuthal angle at the magnetic equatorial plane (where $\phi=0$ aligns with noon), with the 147 empirical shielding exponent $\gamma = 2$ as suggested by previous studies (e.g., Maynard and Chen 148 (1975) and Korth et al. (1999)), $a = 92.4 \text{kV R}_E$ and $b = \frac{0.045}{(1 - 0.159K_p + 0.0093K_n^2)^3} (kV/R_E^2)$ (Maynard 149 and Chen, 1975). Based on the SAPS statistical properties measured by ground-based radar (Foster 150 and Vo, 2002), the magnetospheric SAPS potential model of Goldstein et al. (2005) is given by 151 $\Phi_S(r,\phi,t) = -F(r,\phi)G(\phi)V_S(t)$, where Φ_S describes a potential drop with a time-dependent 152 magnitude $V_S(t) = (0.75kV)K_p^2$. The radial width and radial location of the potential drop are 153 by $F(r,\phi) = \frac{1}{2} + \frac{1}{\pi} \tan^{-1} \left[\frac{4}{\alpha} \{ r - R_S(\phi) \} \right],$ where $R_S(\phi) =$ controlled 154 $R_0 \left[\frac{1+\beta}{1+\beta\cos(\varphi-\pi)} \right]^{\kappa}$ determines SAPS radial location; $\beta = 0.97$, $\kappa =$ 155 $R_0/R_E = 4.4 - 0.6(K_p - 5)$, R_E is the radius of the Earth; $\alpha = 0.15 + (2.55 - 0.27K_p)[1 + (2.55 - 0.27K_p)]$ 156 $\cos\left(\varphi - \frac{7\pi}{12}\right)$] governs the SAPS radial width. $G(\phi)$ governs the variation of potential drop across 157 local time. Both the VS and SAPS models are originally driven by the Kp index; however, we used 158 the Hp index instead of Kp in this study since Hp has a half-hour time cadence while Kp only 159 varies every 3 hours. During storm time, especially in the case of fast injections, it is important to 160 account for faster variations than the 3-hour time cadence given by Kp index. Hence, Hp index is 161 more useful in the present case. 162

Figure 2(a) also shows the variations of radial electric fields calculated using the VS model (blue curve) and a combined VS and Goldstein et al. (2005)'s SAPS model (hereafter referred to as G05 model; green curve) along the Probe - A trajectory during 18:15 UT to 21:15 UT. The VS model does not capture the enhanced radial electric field observations. The G05 model does

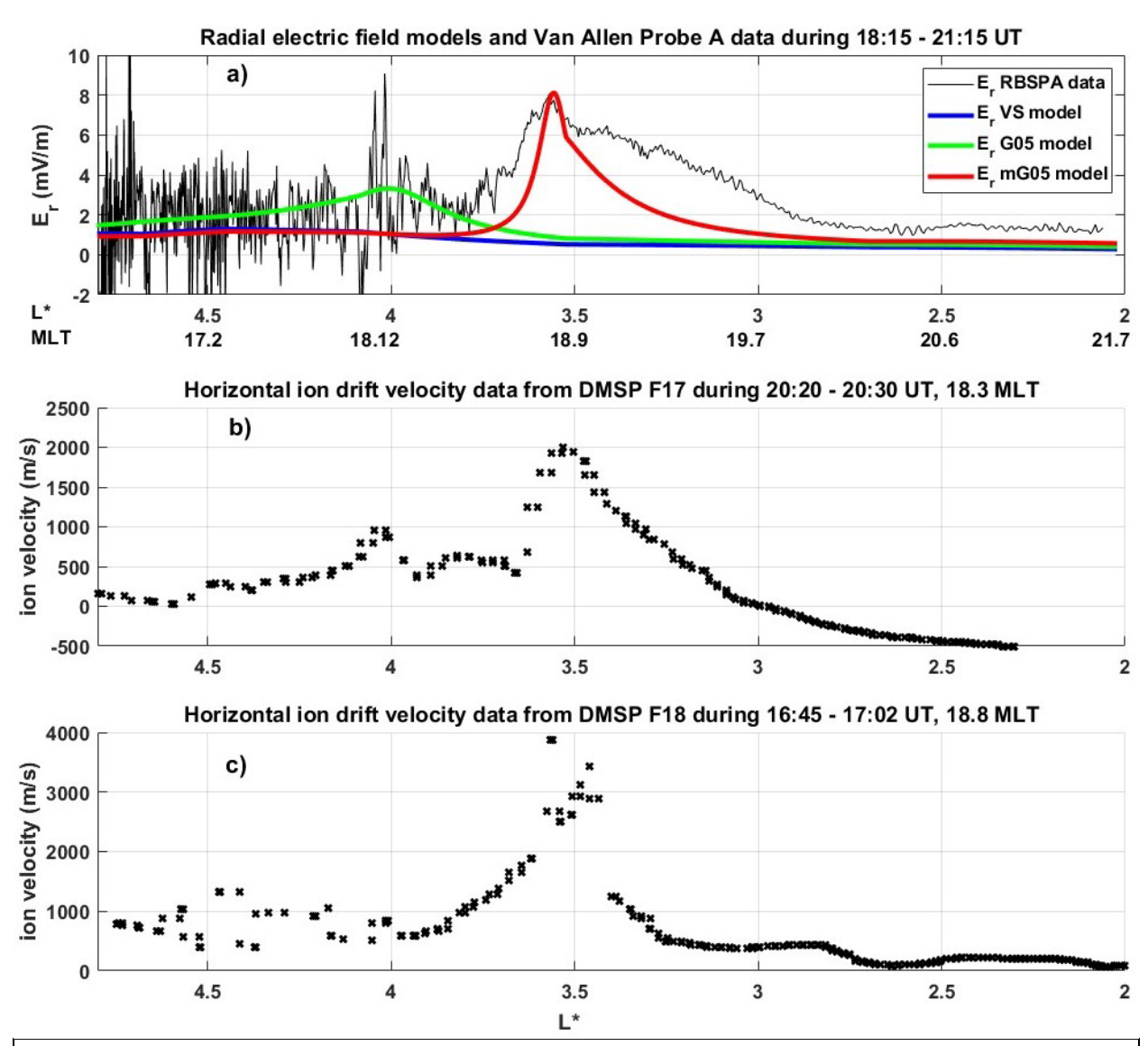


Figure 2 (a) The radial electric fields plotted using Van Allen Probe A observations on 2015-09-07 during 18:15 – 21:15 UT (black curves), using Volland-Stern convection model (blue curve); combined Volland-Stern and SAPS (G05) model (green curve); combined Volland-Stern and modified SAPS (mG05) model (red curve) (b) DMSP F17 observations of horizontal ion drift velocities during 20:20 – 20:30 UT, 18.3 MLT (c) DMSP F18 observations during 16:45 – 17:02 UT, 18.8 MLT.

present an enhanced radial electric field but at a higher L* than the observed electric field enhancement and with a lower amplitude. To better capture the observed SAPS electric field, a modification to the G05 model is made, shown as a combined VS and modified SAPS model (hereafter referred to as mG05; red curve) in Figure 2(a).

The quantitative modifications to the G05 model have been done minimally by keeping the peak potential drop, temporal dependence $V_S(t)$ and azimuthal variation $G(\phi)$ the same, while including an inward shift of the radial location of SAPS (R_0) and narrowing the radial width of SAPS (α) . The modified forms of the equations can thus be written as:

$$R_0/R_E = 3.13 - 0.6(H_p - 5) \tag{1}$$

178
$$= 0.15 + \frac{\left(2.55 - 0.27H_p\right)\left[1 + \cos\left(\varphi - \frac{7\pi}{12}\right)\right]}{8.8}$$
(2)

By using the above modified equations in G05 model, we see an enhancement in the modeled radial electric field (red curve in Figure 2(a)) that quantitatively captures the observed radial electric field enhancement.

Figure 3 shows the contour plots representing the equatorial magnetospheric electrostatic potential variations using VS, SAPS, and modified SAPS models for extreme geomagnetic conditions (Hp = 7). The black circle shows $L^* = 4$ and the red circle presents the geosynchronous orbit ($L^* = 6.6$). Figure 3(a) shows the VS potential representing composite convection and corotation potentials which presents some flow stagnations around the dusk region. Figure 3(b) shows the equipotential lines using the SAPS model, which presents the most significant potential drop around dusk. Figure 3(c) shows the modified SAPS model. As a result of the modifications (Equations (1) and (2)), the closely spaced equipotential lines (corresponding to strong electric fields), which occur inside $L^* = 4$ at dusk in the original model (Figure 3(b)), now appear closer to Earth ($L^* \sim 2$) in the dusk-midnight region. The maximum potential drop to around -35 kV, which occurs at $L^* > 4$ in the original model, occurs as close to Earth as $L^* \sim 3.2$ with the modified model. Figure 3(d) illustrates that incorporating the SAPS potential into the VS model notably amplifies the sunward flow component on the duskside while modifying the flow streamlines

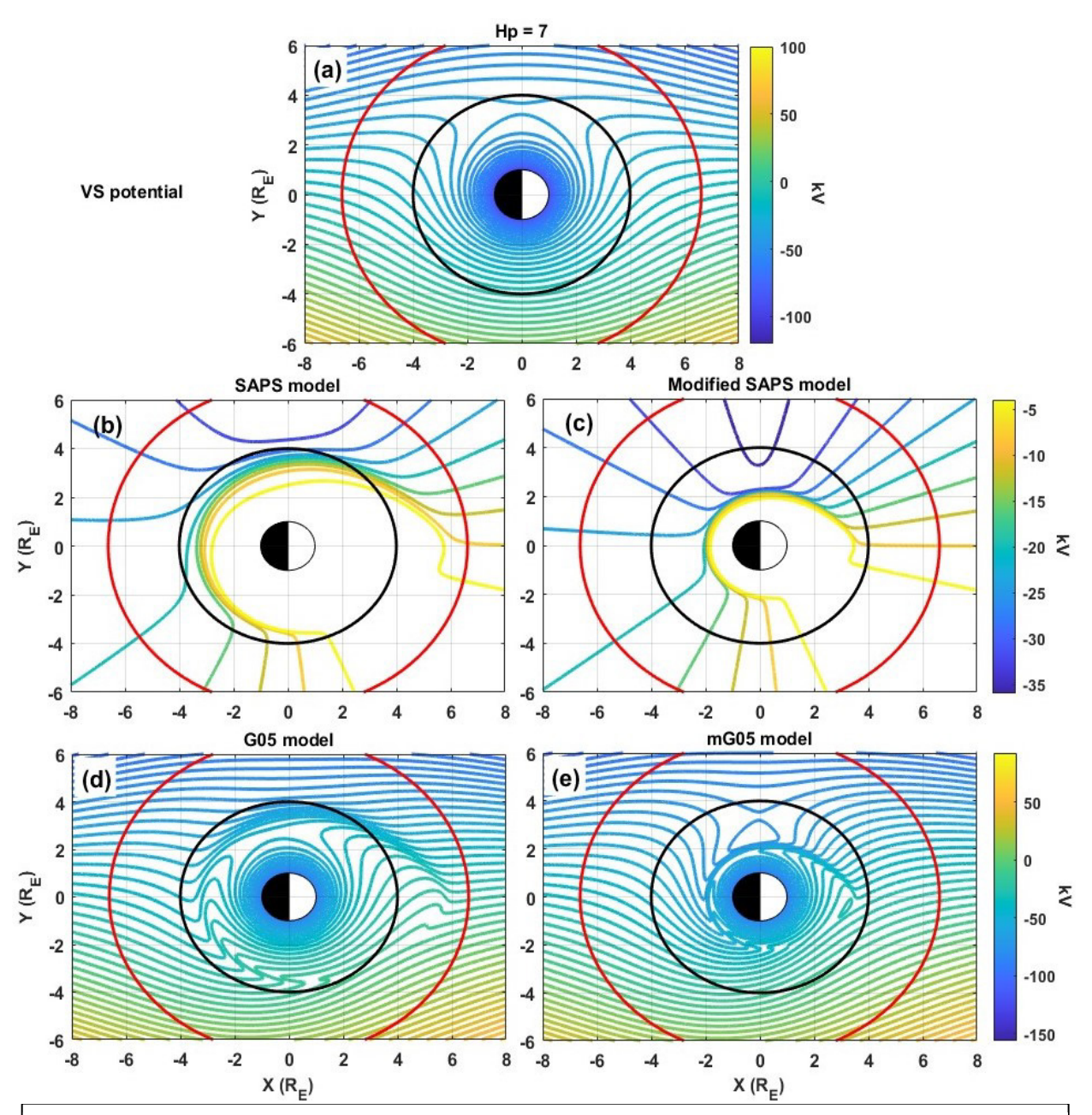


Figure 3 Magnetospheric equatorial potentials for extreme geomagnetic conditions (Hp = 7) using (a) Volland-Stern model (b) SAPS model (c) modified SAPS model (d) combined Volland-Stern and SAPS (G05) model, and (e) combined Volland-Stern and modified SAPS (mG05) model. The black circle in each panel presents $L^* = 4$ and red circle presents $L^* = 6.6$.

Figure 4 shows the global maps of the SAPS radial electric fields during deep injections from 14:00 UT to 17:00 UT. The top panel in Figure 4 shows the electric fields calculated using the original SAPS model, and the bottom panel shows the same using the modified SAPS model. As the original model depicts, evolving from moderate (Figure 4(a)) to extreme geomagnetic storm conditions(Figure 4(d)), the SAPS radial electric field gets stronger and closer to Earth, with the maximum electric field being ~ 11 mV/m. This maximum occurs around the

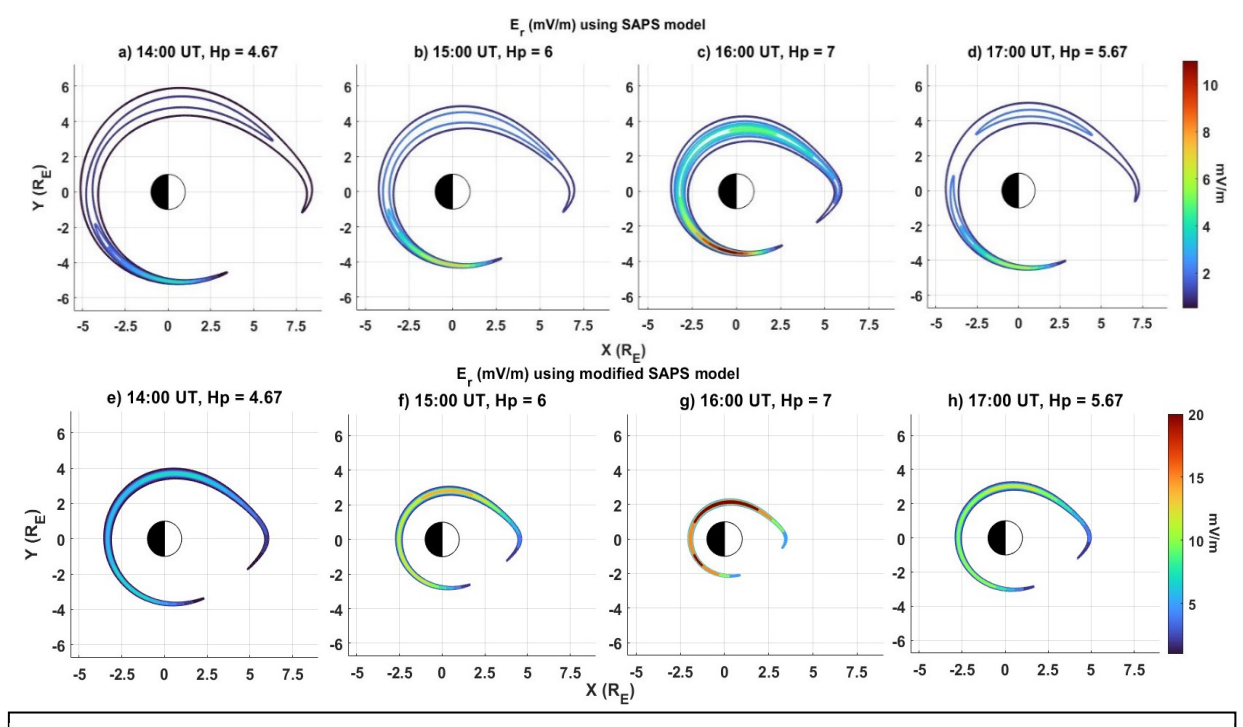


Figure 4 The temporal variation of global map of radial electric field due to SAPS model (a-d) and modified SAPS model (e-h) during 14:00 - 17:00 UT on 2015-09-07.

dawn sector at 16:00 UT with Hp = 7 at L* \sim 3.5 (Figure 4(c)). Another local maximum of lower amplitude \sim 5 mV/m also appears close to dusk in Figure 4(c). On the other hand, the radial electric field using modified SAPS not only shifts to smaller radial locations, but the radial width of the SAPS flow channel is also scaled down. The modified SAPS model also depicts a larger magnitude of radial electric field (up to \sim 20 mV/m) spread over a larger MLT region around dusk (Figure 4(g)). The peak radial electric field inherited from original SAPS model also appears in Figure 4(g) around post-midnight. The corresponding temporal variations of azimuthal electric field has also been shown in the supporting information.

4. Test-Particle Tracing Simulation

In this study, we use a test particle-tracing model to simulate the electron PSD variations. An equatorial 2-D guiding-center code is used to trace 10⁴ electrons of a specific μ value. The total velocity of the particle guiding center is given by

$$v = \mu \frac{B \times \nabla B}{qB^2} + \frac{E \times B}{B^2} \tag{3}$$

here B is the dipole magnetic field of Earth and E is the electric field given by different models, and q is the charge of the electron.

We have used the VS, G05, and mG05 models to simulate their effects on electrons. For the energy range 10s-100s keV, we consider $\mu=10$ MeV/G, 20 MeV/G, 30 MeV/G electrons. The initial PSDs are taken from Van Allen Probe - A measurements right before the deep injection. The simulation time is set to 2.5 hours based on the approximate time difference between the consecutive outbound passes by Probes A and B. The initial location of an electron is randomly chosen by the code between L*=2 and L*=5, the trajectory of each electron is calculated, and the PSD is conserved along the trajectory assuming no source or loss process. The results present the simulated PSDs as a function of L* calculated at spacecraft locations (averaged over a 0.1 L* and 0.4 MLT bin).

5. Results

Figure 5 shows the observed PSD (averaged in L* bins of size $0.1L^*$) before (dotted-dashed red lines) and after (dotted-dashed black lines) the deep injection event for each electron population with a specific μ . The solid colored lines present the simulation results at spacecraft locations calculated using different electric field models. The VS model (blue curves) causes minimum inward transport of electrons of different μ 's. The 10 MeV/G electrons (panel (a)) are pushed to L* as low as ~2.8 using G05 model (green curves), but the electric field generated using mG05 model (red curves) causes 10 MeV/G electrons to move more inward to L* ~ 2.7, closer to the observed innermost enhancement (L*~2.6). At L*>~3.2, the mG05 model produces similar results to the G05 model. The G05 model transports the 20 MeV/G electrons (panel (b)) to L*~2.9. These 20 MeV/G electrons are pushed to L* ~ 2.8 by the mG05 electric field. At 30 MeV/G, none of the models have much impact on radial transport (panel (c)).

- In terms of the PSD enhancements, the VS model produces minimal PSD enhancements. The G05
- 241 model produces some PSD enhancements, which are more significant for 10 MeV/G electrons at
- $L^* \sim 2.9 3.6$ (panel (a)). The electric field generated using the mG05 model causes up to five
- 243 times larger PSD enhancements of 10 MeV/G electrons at $L^* \sim 3 3.3$ and significant PSD
- enhancements of 20 MeV/G electrons (panel (b)) at $L^* \sim 2.9 3.5$, which even completely captures
- the PSD enhancements of 20 MeV/G electrons at L* $\sim 2.85 2.95$.
- Overall, including SAPS electric fields causes more realistic injections, especially at lower
- energies (10 MeV/G), and fitting the SAPS model to observations causes the model to better match
- the particle observations. These results suggest that SAPS play a major role in the deep injections
- of 10s 100s keV electrons, and the modified SAPS model inspired by SAPS observations
- produces larger electron PSD enhancements at low L* than the original SAPS model.

251 6. Discussion

- 252 While the main indicator of SAPS in the equatorial magnetosphere is a robust radial electric field,
- 253 there are concurrent azimuthal electric fields on the eastern and western sides of the SAPS region.
- 254 These azimuthal electric fields lead to inward charged particle transport on the dawn side and
- outward transport on the dusk side. In addition, the effect of SAPS electric fields is drift-phase
- dependent, which may result in a PSD enhancement at one MLT location and a PSD decrease at
- 257 the other. So, we also calculated the averaged PSD across all MLTs in the simulation. The results,
- shown in the supplementary information, still show overall PSD enhancements at low L*,
- indicating that the net effect of SAPS electric fields is to push electrons inwards into lower L*.
- This is likely due to the steep radial gradient in electron PSD, as shown in Figure 5.

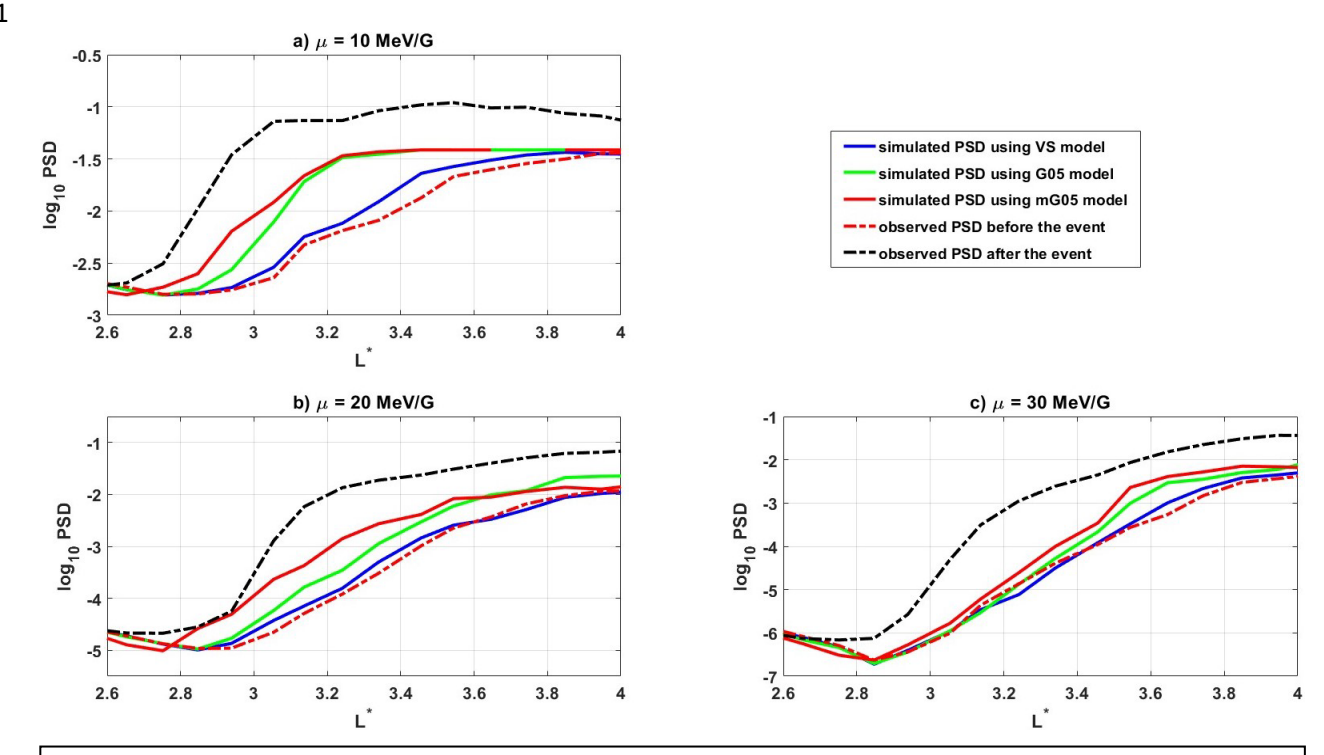


Figure 5 The radial profiles of simulated PSD as a function of L* using three different models for electrons with (a) $\mu = 10$ MeV/G (b) $\mu = 20$ MeV/G (c) $\mu = 30$ MeV/G at the spacecraft locations. The observational PSDs before and after the deep injection event are shown by dashed-dotted lines in each panel.

Although the modified model produces more significant injections compared to the original models, it does not fully reproduce the observed PSD enhancements during the deep injection event. Also, it is inferred that SAPS does not appear to be an important mechanism to transport 30 MeV/G electrons across L*. One possible reason is that the actual electric field strength which caused this deep penetration was stronger, since the Volland-Stern model may underestimate the convection electric field magnitude (the results with a modified Volland-Stern model together with the modified SAPS model are presented in the supplementary information, and the deep injections of 10 and 20 MeV/G electrons are largely reproduced), and/or the temporal electric field variation may be more dynamic than that described by Hp30 index. Another potential reason is that we did not consider the source process in the present study. During geomagnetic disturbances, such as substorms triggered by interactions between the solar wind and the Earth's magnetic field, plasma sheet electrons are injected into the inner magnetosphere. Such injections may significantly increase the PSD of low-energy electrons in the intermediate L*, such as those shown in Figure 5(a) for 10 MeV/G electrons at L*~3.2 and above. Our future studies will include the plasma sheet

- source and we will also consider modifying the VS model to further improve the composite model
- 277 qualitatively as well as quantitatively.

278 Acknowledgements

- 279 This work is supported by NSF AGS 2140934 and NASA 80NSSC22K0356. We acknowledge the
- Van Allen Probes MagEIS team for the use of their data. We also acknowledge the Auburn
- University Easley Cluster for support of this work. H. Zhao thanks Xinlin Li and Yang Mei (LASP,
- 282 CU Boulder) for thoughtful discussions. S. Califf thanks Liam Kilcommons (CIRES,
- NOAA/NCEI) for assisting with interpreting the DMSP data.

Data Availability Statement

- 285 Hp30 index is available from the GFZ website (https://www.gfz-potsdam.de/en/hpo-index,
- Yamazaki et al., 2022); Kp index is also available from the GFZ website (https://www.gfz-
- potsdam.de/en/kp-index/, Matzka et al. 2021). Van Allen Probes (MagEIS) data are publicly
- available at https://rbsp-ect.newmexicoconsortium.org/science/DataDirectories.php (Blake et al.,
- 289 2013; Claudepierre et al., 2021). The DMSP data is available at http://cedar.openmadrigal.org and
- see Rich (1994) for data publication. All the simulation as well as observational data used in the
- 291 present work are available in Goyal et al., (2024).

292293

284

294 References

- 295 Baker, D. N., Lanzerotti, L. J. (2016), Space weather. Am. J. Phys. 84, doi.org/10.1119/1.4938403.
- Blake, J. B., Carranza, P. A., Claudepierre, S. G., Clemmons, J. H., Crain, Jr, W. R., Dotan, W.
- 297 R., et al. (2013). The magnetic electron ion spectrometer (MagEIS) instruments aboard the
- radiation belt storm probes (RBSP) spacecraft. Space Science Reviews, 179, 383–421. https://doi.
- 299 org/10.1007/s11214-013-9991-8.
- Califf, S., Li, X., Blum, L., Jaynes, A., Schiller, Q., Zhao, H., & Bonnell, J. W. (2014). THEMIS
- 301 measurements of quasi-static electric fields in the inner magnetosphere. Journal of Geophysical
- Research: Space Physics, 119(12), 9939–9951. https://doi.org/10.1002/2014JA020360.
- Califf, S., Li, X., Zhao, H., Kellerman, A., Sarris, T. E., Jaynes, A., & Malaspina, D. M. (2017),
- The role of the convection electric field in filling the slot region between the inner and outer
- radiation belts. Journal of Geophysical Research: Space Physics, 122(2), 2051–2068.
- 306 https://doi.org/10.1002/2016JA023657.

- Califf, S., Zhao, H., Gkioulidou, M., Manweiler, J. W., Mitchell, D. G., & Tian, S. (2022), Multi-
- event study on the connection between subauroral polarization streams and deep energetic particle
- injections in the inner magnetosphere. Journal of Geophysical Research: Space Physics, 127,
- 310 e2021JA029895 https://doi.org/10.1029/2021JA029895.
- Claudepierre, S. G., Blake, J. B., Boyd, A. J., Clemmons, J. H., Fennell, J. F., Gabrielse, C., et al.
- 312 (2021), The magnetic electron ion spectrometer: A review of on-orbit sensor performance, data,
- operations, and science. Space Science Reviews, 217(8), 80. https://doi.org/10.1007/s11214-021-
- 314 00855-2.
- 315 Chen, Y., R. Friedel, G. Reeves, T. Onsager, and M. Thomsen (2005), multi-satellite determination
- of the relativistic electron phase space density at the geosynchronous orbit: Methodology and
- initial results in magnetic quiet times, J. Geophys. Res., 110, A10210, doi:10.1029/2004JA010895.
- 318
- Foster, J. C. (1993), Storm time plasma transport at middle and high latitudes. Journal of
- 320 Geophysical Research, 98(A2), 1675–1689. https://doi.org/10.1029/92JA02032.
- 321
- Foster, J. C., & Burke, W. J. (2002), SAPS: A new categorization for sub-auroral electric fields.
- 323 Eos AGU Transactions, 83, 393–394. https://doi.org/10.1029/2002eo000289.
- 324
- Foster, J. C., & Vo, H. B. (2002), Average characteristics and activity dependence of the subauroral
- 326 polarization stream. Journal of Geophysical Research, 107(A12), 1475–1.
- 327 https://doi.org/10.1029/2002JA009409.
- 328
- Galperin, Y, Y N. Ponomarev, and A. G. Zosimova, Plasma convection in the polar ionosphere,
- 330 Ann. Geophys., 30,1,1974.
- 331
- Goldstein, J., Burch, J. L., & Sandel, B. R. (2005), Magnetospheric model of subauroral
- 333 polarization stream. Journal of Geophysical Research, 110, A09222.
- 334 https://doi.org/10.1029/2005JA011135.
- 335
- Goyal, R., Zhao, H., & Califf, S. (2024), Database of "Role of Subauroral Polarization Streams in
- Deep Injections of Energetic Electrons into the Inner Magnetosphere" [Dataset]. Zenodo.
- 338 https://doi.org/10.5281/zenodo.11206586.
- 339
- 340 Hua, M., Li, W., Ma, Q., Ni, B., Nishimura, Y., Shen, X.-C., & Li, H.(2019). Modeling the electron
- flux enhancement and butterfly pitch angle distributions on L shells < 2.5. Geophysical Research
- 342 Letters, 46, 10,967 10,976. https://doi.org/10.1029/2019GL08482.
- 343
- Kanekal, S. G., Baker, D. N., Fennell, J. F., Jones, A., Schiller, Q., Richardson, I. G., et al. (2016).
- Prompt acceleration of magnetospheric electrons to ultrarelativistic energies by the 17 March 2015
- interplanetary shock. Journal of Geophysical Research: Space Physics, 121(8), 7622–7635.
- 347 https://doi.org/10.1002/2016JA022596.
- 348

- Kessel, R. L., N. J. Fox, and M. Weiss (2013), The Radiation Belt Storm Probes (RBSP) and space
- weather, Space Sci. Rev., 179(1-4), 531–543, doi:10.1007/s11214-012-9953-6.

- Korth, H., Thomsen, M. F., Borovsky, J. E., & McComas, D. J. (1999). Plasma sheet access to
- 353 geosynchronous orbit. Journal of Geophysical Research: Space Physics, 104(A11), 25047–25061.
- 354 https://doi.org/10.1029/1999JA900292.

355

- Lejosne, S., Kunduri, B. S., Mozer, F. S., & Turner, D. L. (2018). Energetic electron injections
- deep into the inner magnetosphere: A result of the subauroral polarization stream (SAPS) potential
- drop. Geophysical Research Letters, 45(9), 3811–3819. https://doi.org/10.1029/2018GL077969.

359

- Li, X., Roth, I., Temerin, M., Wygant, J. R., Hudson, M. K., & Blake, J. (1993). Simulation of the
- prompt energization and transport of radiation belt particles during the March 24, 1991 SSC.
- Geophysical Research Letters, 20(22), 2423–2426. https://doi.org/10.1029/93GL02701.

363

- Lyons, L. R., and R. M. Thorne (1973), Equilibrium structure of radiation belt electrons, J.
- 365 Geophys. Res., 78(13), 2142–2149, doi:10.1029/JA078i013p02142.

366

- Matzka, J., Stolle, C., Yamazaki, Y., Bronkalla, O., & Morschhauser, A. (2021). The geomagnetic
- 368 Kp index and derived indices of geomagnetic activity. Space Weather, 19, e2020SW002641.
- 369 https://doi.org/10.1029/2020SW002641.

370

- Mauk, B., N. Fox, S. Kanekal, R. Kessel, D. Sibeck, and A. Ukhorskiy (2012), Science objectives
- and rationale for the radiation belt storm probes mission, Space Sci. Rev., 179, 3-27,
- 373 doi:10.1007/s11214-012-9908-y.
- Maynard, N. C., & Chen, A. J. (1975). Isolated cold plasma regions: Observations and their
- 375 relation to possible production mechanisms. Journal of Geophysical Research, 80(7), 1009–1013.
- 376 https://doi.org/10.1029/JA080i007p01009.
- 377 Millan, R. M., and D. N. Baker (2012), Acceleration of particles to high energies in Earth's
- 378 radiation belts, Space Sci. Rev., 173, 103–131, doi:10.1007/s11214-012-9941-x.

379

- Reeves, G. D., Friedel, R. H. W., Larsen, B. A., Skoug, R. M., Funsten, H. O., Claudepierre, S.
- 381 G.,...Baker, D. N. (2016), Energy-dependent dynamics of keV to MeV electrons in the inner zone,
- outer zone, and slot regions. Journal of Geophysical Research: Space Physics, 121, 397–412.
- 383 https://doi.org/10.1002/2015JA021569.

384

- Rich, F. J. (1994), Users guide for the topside ionospheric plasma monitor (SSIES. SSIES-2 AND
- 386 SSIES-3) on spacecraft o the Defense Meteorological Satellite Program (DMSP), Vol. I,
- 387 https://apps.dtic.mil/sti/citations/ADA315731.

388

- Rowland, D. E., & Wygant, J. R. (1998), Dependence of the large-scale, inner magnetospheric
- electric field on geomagnetic activity. Journal of Geophysical Research: Space Physics, 103(A7),
- 391 14959–14964. https://doi.org/10.1029/97JA03524.

392

- 393 Spiro, R.W, R. A. Heelis, and W B. Hanson, Rapid subauroral ion drifts observed by Atmospheric
- 394 Explorer C, Geophys. Res. Lett., 6,657-660,1979.

Stern, D. P. (1975). The motion of a proton in the equatorial magnetosphere, Journal of Geophysical Research, 80, 595–599. https://doi.org/10.1029/JA080i004p00595.

398

- 399 Su, Y. J., Selesnick, R. S., & Blake, J. B. (2016), Formation of the inner electron radiation belt by
- 400 enhanced large-scale electric fields. Journal of Geophysical Research: Space Physics, 121(9),
- 401 8508-8522. https://doi.org/10.1002/2016JA022881.

402

Tsyganenko, M. (1989), A magnetospheric magnetic field model with a wrapped tail current sheet, Planet. Space Sci., 37, 5–20.

405

- Turner, D. L., Claudepierre, S. G., Fennell, J. F., O'Brien, T. P., Blake, J. B., Lemon, C., et al. (2015). Energetic electron injections deep into the inner magnetosphere associated with substorm
- 408 activity. Geophysical Research Letters, 42, 2079–2087. https://doi.org/10.1002/2015GL063225.

409

Volland, H. (1973). A semiempirical model of large-scale magnetospheric electric fields. Journal of Geophysical Research, 78, 171–180. https://doi.org/10.1029/JA078i001p00171.

412

- Wygant, J. R., Bonnell, J. W., Goetz, K. et al. The Electric Field and Waves Instruments on the
- 414 Radiation Belt Storm Probes Mission. Space Sci Rev, 179, 183–220 (2013).
- 415 https://doi.org/10.1007/s11214-013-0013-7.

416

- Yamazaki, Y., Matzka, J., Stolle, C., Kervalishvili, G., Rauberg, J., Bronkalla, O., et al. (2022).
- Geomagnetic activity index Hpo. Geophysical Research Letters, 49, e2022GL098860. https://doi.
- 419 org/10.1029/2022GL098860.

420

Yeh, H.-C, J. C. Foster, F J. Rich, and W Swider, Stormtime electric field penetration observed at midlatitude, J Geophys. Res., 96,5707,1991.

423

- Zhao, H., Baker, D. N., Califf, S., Li, X., Jaynes, A. N., Leonard, T., et al. (2017). Van Allen
- 425 probes measurements of energetic particle deep penetration into the low L region (L \leq 4) during
- 426 the storm on 8 April 2016. Journal of Geophysical Research: Space Physics, 122(12), 140–12,152.
- 427 https://doi.org/10.1002/2017JA024558.

428

- Zhao, H., Califf, S. T., Goyal, R., Li, X., Gkioulidou, M., Manweiler, J. W., & Krantz, S. (2023).
- 430 Statistical analysis of the differential deep penetration of energetic electrons and protons into the
- low L region (L < 4). Journal of Geophysical Research: Space Physics, 128, e2022JA031125.
- 432 https://doi. org/10.1029/2022JA031125.